NASA Technical Memorandum 85697

STABILITY, VIBRATION, AND PASSIVE DAMPING OF PARTIALLY RESTRAINED IMPERFECT COLUMNS

Zia Razzaq, R. T. Voland, H. G. Bush and M. M. Mikulas, Jr.

October 1983

National Aeronautics and Space Administration

Langley Research Center
Hampton, Virginia 23665

STABILITY, VIBRATION, AND PASSIVE DAMPING OF PARTIALLY RESTRAINED IMPERFECT COLUMNS

Z. Razzaq
Department of Civil Engineering
Old Dominion University
Norfolk, Virginia

R. T. Voland, H. G. Bush, and M. M. Mikulas, Jr.
Langley Research Center

SUMMARY

A theoretical and experimental study of slender tubular columns for possible use in space structures is conducted in the presence of partial rotational end restraints. New explicit formulas are derived for computing the buckling load and the lowest natural frequency of perfectly straight uniform elastic members with rotational end restraints possessing linear moment-rotation characteristics. An exact solution in the form of a transcendental equation, and a numerical solution using second-order finite-differences are also presented. The presence of an initial imperfection is also incorporated into the numerical procedure. Each of the solutions presented originates from the partial differential equation and the associated boundary conditions for the problem. It is shown that the buckling load and the natural frequency formulas developed are highly accurate. Vibration tests are conducted on an imperfect tubular steel member in the absence of an axial load. A damping concept consisting of a string-mass assembly is explored in a few of the tests, in addition to the structural damping present in the system. Three passive damping configurations were investigated; one with three small equidistant lead shots attached to a string inside the tubular member, one with the three lead shots attached at the center of the tube, and the other with one lead shot at the center of the tube. The three lead shot configurations both provided considerably greater damping than the single lead shot damper.

SYMBOLS

C	damping coefficient
D_o	outer diameter of the tubular member
E	Young's modulus
f	lowest natural frequency of the column
f_e	experimental natural frequency
$\bar{f}$	dimensionless natural frequency
h	panel length
I	moment of inertia
K	end rotational stiffness
$\bar{K}$	dimensionless end rotational stiffness
L	member length
P	axial load
P_{cr}	buckling load of the column
$\bar{P}$	dimensionless buckling load of the column
t	time
t_o	wall thickness of the tubular member
w	net lateral displacement
$\bar{w}$	initial out-of-straightness
x	member longitudinal ordinate
y	axis parallel to the face of the proximity probe
z	axis perpendicular to the face of the proximity probe
Δ	envelope of the midspan maximum dynamic deflection
Δt	time interval
ζ	damping ratio
ρ	mass per unit length of the column

INTRODUCTION

The analysis for buckling and natural vibration of elastic columns with pinned or fixed end conditions is well-known (see refs. 1 and 2). The practical columns in real space structures, however, seldom possess such ideal boundary conditions. The connections and the adjoining members which frame in at the ends of a typical column in a space structure provide rotational restraints which affect the behavior of the column itself. The buckling load of a partially restrained column may be obtained by using the classical eigenvalue approach leading to a transcendental equation (see for example, ref. 3) which must be solved iteratively. Also, it is possible to formulate an exact solution for determining the natural frequency of such a member in the form of a complicated transcendental equation which must also be solved iteratively. This paper presents an outcome of a theoretical and experimental investigation of tubular members restrained partially. New explicit formulas are derived for computing the buckling load and the natural frequency of perfectly straight uniform elastic members having partial rotational end restraints possessing linear moment-rotation characteristics. An exact solution in the form of a transcendental equation, and a numerical solution using second-order finite-differences are also presented. The presence of initial imperfection is also incorporated into the numerical procedure. Each of the solutions presented originates from the partial differential equation of motion governing the dynamic response of the column in the presence of a constant axial load and the boundary conditions representing the rotational springs. The vibration tests are conducted on an imperfect tubular steel member with rotational elastic end restraints and in the absence of an axial load. The use of a damping concept is explored in a few of the tests, in addition to the structural damping already present in the system.

PROBLEM STATEMENT AND GOVERNING EQUATIONS

Figure 1 shows schematically a slender column of length L with a hollow circular cross section. The outer diameter of the section is D_o and the wall thickness is t_o. The column has an initial out-of-straightness given by $\bar{w}$. A static axial load P is applied to the column. Also, the ends of the column are not allowed to translate laterally, and possess partial rotational restraints each having a rotational spring stiffness of K in-lb/radian. The material of the column is elastic. The governing differential equation of equilibrium for the member shown in figure 1 may be written as:

$$EI \frac{\partial^4 w}{\partial x^4} + P\left(\frac{\partial^2 w}{\partial x^2} + \frac{\partial^2 \bar{w}}{\partial x^2}\right) + \rho \frac{\partial^2 w}{\partial t^2} + C \frac{\partial w}{\partial t} = 0 \qquad (1)$$

in which

$w(w,t)$ = lateral displacement

$\bar{w}(x)$ = initial out-of-straightness, or imperfection

EI = flexural rigidity of the column

P = axial load

ρ = mass per unit length of the column

C = damping coefficient

Equation (1) without the term involving $\bar{w}$ can be found in the standard texts on structural dynamics (see, for example, ref. 2). As evident from the last term in equation (1), the system damping is assumed to be proportional to the velocity at any given time.

BOUNDARY AND INITIAL CONDITIONS

The boundary conditions for the problem shown in figure 1 are as follows:

$$w(0,t) = 0 \qquad (2)$$

$$w(L,t) = 0 \qquad (3)$$

$$EI \frac{\partial^2 w}{\partial x^2}(0,t) = K \frac{\partial w}{\partial x}(0,t) \tag{4}$$

$$EI \frac{\partial^2 w}{\partial x^2}(L,t) = -K \frac{\partial w}{\partial x}(L,t) \tag{5}$$

Equations (2) and (3) represent zero lateral translation of the member ends. Equations (4) and (5) are the natural boundary conditions dependent upon the flexural stiffness of the column ends and the restraint moments developed by the rotational springs.

The initial conditions for obtaining the natural frequency of the column are taken as follows:

$$w(x,0) = \phi(x; P, K, EI, L) \tag{6}$$

$$\frac{\partial w}{\partial t}(x,0) = 0 \tag{7}$$

in which ϕ is a function of x and the terms P, K, EI, and L. The initial condition given by equation (6) states that at time t equal to zero, the column has been displaced ("plucked") resulting in a shape given by a function of x, the applied axial load P, the spring constant K, the flexural rigidity EI, and the length L. Equation (7) imposes a zero initial velocity condition.

EXACT SOLUTION

For the case of no initial imperfection, that is, $\bar{w} = 0$, equation (1) can be solved by the separation of variables technique by letting:

$$w(x,t) = W(x)\, T(t) \tag{8}$$

Substituting equation (8) into (1) leads to the following pair of ordinary differential equations (see ref. 4):

$$\frac{d^4W}{dx^4} + k^2 \frac{d^2W}{dx^2} - \lambda W = 0 \tag{9}$$

$$\frac{d^2T}{dt^2} + \frac{C}{\rho} \frac{dT}{dt} + \omega^2 T = 0 \tag{10}$$

in which λ is a parameter to be determined, ω is the undamped circular frequency given by:

$$\omega = \sqrt{\frac{EI\lambda}{\rho}} \tag{11}$$

and k is given by:

$$k = \sqrt{\frac{P}{EI}} \tag{12}$$

The exact solution to equation (9) is given by (ref. 4):

$$W(w) = B_1 \cos \beta_1 x + B_2 \sin \beta_1 x + B_3 \cosh \beta_2 x + B_4 \sinh \beta_2 x \tag{13}$$

in which

$$\beta_{1,2}^2 = \pm \frac{k^2 \pm \sqrt{k^4 + 4\lambda}}{2} \tag{14}$$

and B_1 through B_4 are constants of integration. The solutions to equation (10) are all of the form (ref. 6):

$$T = F(t) \tag{15}$$

in which $F(t)$ depends upon the problem input parameters, ω, and the initial conditions (6) and (7) invoked via equation (8). The damped circular frequency, ω_d, is given by (ref. 6):

$$\omega_d = \omega\sqrt{1 - \zeta^2} \tag{16}$$

in which ζ is the damping ratio.

The solutions based on equation (13) for idealized pinned or fixed end conditions are given in the literature (see ref. 4). Here, an exact solution for a column with partial restraints and having the boundary conditions given by equations (2) through (5) is presented. Using equation (8), these conditions reduce to the following ones:

$$W(0) = 0 \tag{17}$$

$$W(L) = 0 \tag{18}$$

$$EI \frac{d^2W}{dx^2}(0) = K \frac{dW}{dx}(0) \tag{19}$$

$$EI \frac{d^2W}{dx^2}(L) = -K \frac{dW}{dx}(L) \tag{20}$$

Substituting equation (13) into equations (17) through (20) results in a matrix equation of the type:

$$\begin{bmatrix} a_{11} & a_{12} & a_{13} & a_{14} \\ a_{21} & a_{22} & a_{23} & a_{24} \\ a_{31} & a_{32} & a_{33} & a_{34} \\ a_{41} & a_{42} & a_{43} & a_{44} \end{bmatrix} \begin{Bmatrix} B_1 \\ B_2 \\ B_3 \\ B_4 \end{Bmatrix} = \begin{Bmatrix} 0 \\ 0 \\ 0 \\ 0 \end{Bmatrix} \tag{21}$$

in which the a_{ij} terms are given in appendix A. Setting the determinant of the matrix in equation (21) equal to zero leads to a complicated transcendental equation. For a given value of the axial load P, the column dimensions and material properties, and the spring constant K, the resulting transcendental equation may be solved iteratively for the lowest nontrivial value of λ. A substitution of this λ value into equation (11) gives the circular frequency of the partially restrained column. To find the column static buckling load,

however, the smallest nontrivial value of P must be sought with $\lambda = 0$, since the frequency of a column becomes zero when the axial static load equals the buckling load.

When the axial load P is less than the buckling load, the deflection versus time relationship may be found by substituting the ω value, ascertained by the iterative procedure, into equations (13) and (15) which, in turn, must be substituted into equation (8).

The disadvantage of the exact solution is that it can be obtained only through trial and error. In the following section, explicit formulas for computing the buckling load and the natural frequency of the partially restrained column are derived.

BUCKLING LOAD AND NATURAL FREQUENCY FORMULAS

In this section, new explicit formulas for calculating the buckling load and the natural frequency of the partially restrained column shown in figure 1, in the absence of initial imperfections, are derived and are based on a highly accurate assumed mode shape of the column. The procedure involves selecting a trigonometric expression which satisfies the boundary conditions a priori, and then using Galerkins' orthogonality criterion.

Let the solution to equation (9) be taken in the following form:

$$W = A_1 \sin \frac{\pi x}{L} + A_2\left(1 - \cos \frac{2\pi x}{L}\right) \tag{22}$$

in which A_1 and A_2 are constants. This expression satisfies the boundary conditions (17) and (18). The sine term alone would represent a pinned member while the term in the parentheses approximates a completely fixed end member. A combination of the two functions has not been explored by any previous investigator for simulating the deflected shape of the member with end conditions

somewhere between pinned and fixed cases, that is, for the partially restrained end conditions. Equation (22) represents the approximate fundamental mode of the member, thus the buckling load and the natural frequency expressions are associated with this mode. Furthermore, due to the symmetry of the W expression about the member midspan, it is sufficient to enforce only one of the conditions given by equations (19) and (20). Substituting W from equation (22) into equation (19) results in the following relationship between A_1 and A_2:

$$A_2 = \frac{KL}{4\pi EI} A_1 \tag{23}$$

Substituting equation (23) into (22) gives:

$$W = A_1\left[\sin\frac{\pi x}{L} + \frac{KL}{4\pi EI}\left(1 - \cos\frac{2\pi x}{L}\right)\right] \tag{24}$$

If equation (24) were exact solution, it would satisfy equation (9) exactly. Since it is an approximate solution, its substitution into equation (9) results in an error expression given by ε as follows:

$$\varepsilon = A_1\left\{\frac{\pi^4}{L^4}\left(\sin\frac{\pi x}{L} - 16\eta\cos\frac{2\pi x}{L}\right) + \frac{\pi^2 k^2}{L^2}\left(-\sin\frac{\pi x}{L} + 4\eta\cos\frac{2\pi x}{L}\right)\right.$$
$$\left. - \lambda\left[\sin\frac{\pi x}{L} + \eta\left(1 - \cos\frac{2\pi x}{L}\right)\right]\right\} \tag{25}$$

in which:

$$\eta = \frac{KL}{4\pi EI} \tag{26}$$

Invoking use of Galerkin's orthogonality criterion gives the following equation:

$$\int_0^L \varepsilon\left[\sin\frac{\pi x}{L} + \eta\left(1 - \cos\frac{2\pi x}{L}\right)\right] dx = 0 \tag{27}$$

Upon performing the integration, rearranging, and noting that $A_1 \neq 0$ for the nontrivial solution, an explicit expression for λ is obtained from equation (27). Using this λ expression, and noting that $\omega = 2\pi f$, where f is the undamped natural frequency in Hertz, the following formula is obtained:

$$f = \frac{1}{2L}\sqrt{\frac{EI}{\rho}\left[\frac{12(\pi EI)^2\left(\frac{\pi^2}{L^2} - \frac{P}{EI}\right) + 32\ EIKL\left(\frac{5}{2}\frac{\pi^2}{L^2} - \frac{P}{EI}\right) + 3(KL)^2\left(\frac{4\pi^2}{L^2} - \frac{P}{EI}\right)}{12(\pi EI)^2 + 32\ EIKL + \frac{9}{4}(KL)^2}\right]} \tag{28}$$

Of course, the damped frequency can be obtained by using equation (16).

A buckling load formula for the column shown in figure 1 can be obtained by setting f from equation (28) equal to zero, since the frequency of the column approaches zero as the axial load approaches the buckling load. Thus, setting the right side of equation (28) to zero, simplifying, and solving for the critical P value leads to:

$$P_{cr} = \frac{\pi^2 EI}{L^2}\left[\frac{12(\pi EI)^2 + 80\ EIKL + 12(KL)^2}{12(\pi EI)^2 + 32\ EIKL + 3(KL)^2}\right] \tag{29}$$

Formulas (28) and (29) can be used to predict the natural frequency, and the elastic buckling load of a perfect column with equal partial end restraints.

The formulas derived above are directly applicable in the absence of an initial imperfection. It is well-known (ref. 3) that the maximum load which an imperfect elastic column may carry, in the presence of pinned or fixed end conditions, asymptotically approaches the Euler buckling load of the corresponding perfect member. Although the details are not given here, it can be shown that the same conclusion is applicable to the partially restrained column considered herein. Furthermore, similar reasoning is applicable to the evaluation of the lowest natural frequency of both perfect and imperfect members.

COMPARISON FOR LIMITING BOUNDARY CONDITIONS

If the end spring stiffness K is taken as zero, the limiting case of a column with pinned ends is obtained. It can be verified that if K is set equal to zero in equations (28) and (29), the resulting f and P_{cr} values are the exact solution for pinned ends (see refs. 1, 2, and 5). For a fixed end column, the value of K equals infinity. To evaluate f for this limiting case, the numerator and the denominator terms under the radical sign should first be divided by K^2 and the resulting expression evaluated as K approaches infinity. Using the expression for f thus obtained, the circular frequency ω for a member with zero axial load is found to be as follows:

$$\omega = 22.79\sqrt{\frac{EI}{\rho L^4}} \tag{30}$$

which is only slightly different from the exact ω expression given in reference 5 with a coefficient of 22.40 outside of the radical te~~m~~. To evaluate P_{cr} with an infinite value for K, the numerator and the denominator terms on the right side of equation (29) should first be divided by K^2 and the resulting expression evaluated as K approaches infinity. This process leads to the exact buckling load of a fixed end column given in reference 1.

INTERACTION RELATIONS

Figure 2 presents nondimensional interaction curves relating the nondimensional frequency $\bar{f}$ and its square $(\bar{f})^2$ with no axial load ($P = 0$ in fig. 1), and the buckling load $\bar{P}$, to the nondimensional spring constant $\bar{K}$, defined as follows:

$$\bar{f} = \frac{f}{f_\infty} \tag{31}$$

$$\bar{P} = \frac{P_{cr}}{P_\infty} \tag{32}$$

$$\bar{K} = \frac{K}{EI} \tag{33}$$

in which f is given by equation (28) with $P = 0$; f_∞ is the value of f with $K = \infty$; P_{cr} is given by equation (29); and P_∞ is the value of P_{cr} with $K = \infty$. As seen from this figure, $\bar{f}$ increases from about 0.433 to 1.0 as $\bar{K}$ is varied between zero and infinity. The variation of $(\bar{f})^2$ with $\bar{K}$ is also shown. Similarly, $\bar{P}$ increases from 0.25 to 1.0 as $\bar{K}$ is varied between zero and infinity, viz., from the pinned to the completely fixed end condition. Substantial increases in $\bar{f}$, $(\bar{f})^2$, and $\bar{P}$ occur as $\bar{K}$ is increased from zero to about 20, beyond which only small increases are observed even for very significant increments in $\bar{K}$. This shows that what may appear to be a nominal end restraint may actually provide a considerable degree of end fixity rather than a nearly pinned condition. In fact, a 'moderate' amount of end restraint may provide near-complete end fixity.

As may be seen from equation (28), the presence of an axial load P in the presence of partial end restraints would reduce the natural frequency f. Thus, the $\bar{f}$, and $(\bar{f})^2$ versus $\bar{K}$ relations with $P > 0$ would fall below those shown in figure 2.

A comparison of the $\bar{P}$ versus $\bar{K}$ relation shown in figure 2 was made with a finite element solution of the problem where the column was divided into a total of ten segments. The results were found to be almost identical. The validity of the formula (29) was also verified by computing a few of the points on the $\bar{P}$ versus $\bar{K}$ relation in figure 2 using an exact eigenvalue solution discussed earlier in this paper. Again, the results were almost identical.

FINITE-DIFFERENCE SOLUTION

Using second-order central finite-difference expressions (see ref. 7), the partial differential equation (1) may be written as follows:

$$\frac{EI}{h^4}(w_{i-2,j} - 4w_{i-1,j} + 6w_{i,j} - 4w_{i+1,j} + w_{i+2,j})$$

$$+ \frac{P}{h^2}(w_{i-1,j} - 2w_{i,j} + w_{i+1,j}) + P\phi(x_i)$$

$$+ \frac{\rho}{(\Delta t)^2}(w_{i,j-1} - 2w_{i,j} + w_{i,j+1}) + \frac{C}{(\Delta t)^2}(-w_{i,j} + w_{i,j+1}) = 0 \qquad (34)$$

in which:

h = panel length along the x-axis of the column (fig. 1)

Δt = time interval

$\phi(x_i)$ = second derivative relative to x of the imperfection function $\bar{w}$

$x_i = ih$, for each $i = 1, 2, 3, \ldots$

The subscript i refers to the ith panel point over the domain $0 < x < L$, and the subscript j refers to the number of time increments such that the time at j is given by the following equation:

$$t_j = j(\Delta t), \text{ for each } j = 0, 1, 2, 3, \ldots$$

Similarly, the boundary conditions (2) through (5) can be expressed in the finite-difference form as follows:

$$w_{0,j} = 0 \qquad (35)$$

$$w_{M,j} = 0 \qquad (36)$$

$$\left(\frac{EI}{h} + \frac{K}{2}\right)w_{-1,j} + \left(\frac{EI}{h} - \frac{K}{2}\right)w_{1,j} = 0 \qquad (37)$$

$$\left(\frac{EI}{h} + \frac{K}{2}\right)w_{M-1,j} + \left(\frac{EI}{h} + \frac{K}{2}\right)w_{M+1,j} = 0 \qquad (38)$$

Applying equation (34) at $i = 1, 2, 3, \ldots, (M-1)$ and invoking the conditions (35) through (38) leads to the following matrix equation:

$$\{w_{i,j+1}\} = c_1[r]\{w_{i,j}\} + c_2\{w_{i,j-1}\} + \{p_i\} \tag{39}$$

in which:

$$c_1 = -\frac{1}{b_3 + b_4} \tag{40}$$

$$c_2 = b_3 c_1 \tag{41}$$

$$b_3 = \frac{\rho}{(\Delta t)^2} \tag{42}$$

$$b_4 = \frac{C}{\Delta t} \tag{43}$$

$$p_i = P c_1 \phi(x_i) \tag{44}$$

and $[r]$ is a symmetric coefficient matrix of the order (M-1) by (M-1). Appendix B defines the terms of this matrix for $M = 6$ as an example.

Equation (39) may be used to predict the lateral deflections $w_{i,j+1}$ if $w_{i,j}$ and $w_{i,j-1}$ are known. To avoid having a negative time interval due to the use of the central finite-difference scheme when starting the recursion indicated in this equation, the following special forward start-up difference equation for $w_{i,1}$ is derived in appendix C:

$$w_{i,1} = b_6\phi_{i-2} + (-4b_6 + b_7)\phi_{i-1} + (6b_6 - 2b_7 + 1)\phi_i + (-4b_6 + b_7)\phi_{i+1} + b_6\phi_{i+2} + b_8 p\phi_i \tag{45}$$

in which:

$$b_6 = -\frac{(\Delta t)^2}{2h^4}\frac{EI}{\rho} \tag{46}$$

$$b_7 = -\frac{(\Delta t)^2}{2h^2}\frac{P}{\rho} \tag{47}$$

$$b_8 = -\frac{(\Delta t)^2}{2}\frac{P}{\rho} \tag{48}$$

In using the recursive equation (39), the panel length h and the time increment Δt should be kept small to avoid numerical instability of the solution. For the member tested in the laboratory described later in this paper, it was found sufficient to use $h = L/6$, and $\Delta t = 0.001$ sec to ensure both convergence and numerical stability.

EXPERIMENTAL INVESTIGATION

The experimental portion of the investigation consisted of conducting several natural vibration tests on a tubular steel member of about 12 ft length, and outer and inner diameters of 0.50 and 0.37 in., respectively. The ends were partially restrained by specially designed connections, and no axial load was applied. The steel member was used since very slender graphite composite tubes are not yet available, and the procedures used in this investigation are good for both materials. The member had some initial imperfection due to manufacturing and handling processes.

Figure 3 shows sketches of the member tested, and the details of the end connections. Each end connection was a two-piece assembly. One piece was a steel blade 1-1/2 in. long with a 3/16 in. × 1/2 in cross section welded to a steel base plate. The other piece was a steel clevis designed to fit snugly over all but 1/4 in. of the blade and fastened to it by screws fitted through two drilled holes. The exposed 1/4 in. of the blade, thin in one direction (3/16 in.) but thick in the other (1/2 in.) provided partial rotational restraint in one plane of vibration and almost total rotational restraint in the orthogonal plane. This design provided the member a preferred direction of vibration, namely, about the weaker axis of the blade. The top end of the clevis was a 1-in. threaded rod which screwed into the steel member. The member and the end fixtures were threaded so that one end had right-hand threads and the other had left-hand threads. These opposite thread directions

allowed the system to act like a turnbuckle so that the top and the bottom end fixtures could be easily aligned during assembly. The upper base plate was bolted to a heavy bracket which in turn was bolted to a backstop, and the lower base plate was bolted to the floor directly beneath the upper one. The clevis portions of both end fixtures were screwed into the appropriate ends of the member. The upper end of the member was then attached by the clevis-blade joint to the base plate. The turnbuckle feature of the system was then used to align the attachment holes on the lower end clevis-blade joint so that no axial tension or compression was induced in the system.

The instrumentation used in the tests consisted of a proximity probe, proximity probe target, and a strip chart. The proximity probe was mounted on a bracket at midspan of the tube and in line with the preferred axis of vibration. A flat circular piece of aluminum was bonded to the member at midspan for use as a target for the proximity probe. A photo linagraph strip chart plotted the relative deflection versus time using deflection data from the proximity probe.

Evaluation of End Restraint Stiffness

To evaluate the end restraint rotational stiffness K experimentally, the setup shown schematically in figure 4 was used. The base plate with the clevis-blade joint (a) described earlier is bolted to the test bed. A rigid round steel bar (b) is screwed into the top of the clevis. A cable (c) is attached to the steel bar near its top end and looped around the pulleys d, e, f, g, and connected to the connection blade close to the bottom, as shown in the figure. When a load W is suspended through the pulley f, it introduces equal and opposite forces in the horizontal portions (c and h) of the cable, thus cancelling the shear in the connection and the steel bar between the points of cable attachment while applying a pure bending moment to the clevis-blade

connection. The elimination of the force is necessary since the connection rotational spring stiffness K is the slope of only the pure moment versus the rotation relationship. A dial gage was mounted at 12 in. from the base plate to measure the horizontal deflections of the steel bar b for successive increments in the applied load W. The deflections thus measured were used for computing the connection rotations. The maximum value of W applied was 2.6 lb. Five tests were conducted by attaching the shear-cancelling cable to the lower clevis-blade attachment screw, and another five were conducted by a similar attachment to the upper screw. The same number of tests were also conducted on each of the top and the bottom end fixtures. The average of these 20 tests resulted in a linear moment-rotation relationship from which the following value of K was obtained:

$$K = 1{,}974.3 \text{ in-lb/radian} \tag{49}$$

and was found to be similar to that obtained from approximate theoretical stiffness calculations using simple bending theory.

Natural Vibration Tests

A number of natural vibration tests were conducted on the partially restrained tubular member shown in figure 3 both with and without internal passive damping devices. Figure 5 shows schematically the tubular member with (a) no internal passive damping device; (b) with an internal passive damper in the form of a single lead shot weighing 0.47 gms attached at midheight to a nylon fishing string weighing 0.17 gms which in turn is anchored internally to the fixtures at both ends of the member; (c) a mass-string system with a lead shot at each of the locations 0.25L, 0.50L, and 0.75L from the bottom of the member; and (d) a mass-string system with three lead shots at the member midspan. The same nylon string was used in each arrangement, and each individual

lead shot in arrangements (c) and (d) weighed the same as the one in arrangement (b). The deflection-time plots were obtained by "plucking" the member manually by a small amount either toward or away from the proximity probe at the midheight. The plot generated was used to calculate the frequency of the member, and the system damping. Although no internal passive damper was provided in arrangement (a) the deflection-time relationship exhibited a gradual though slow decay due to the inevitable presence of structural damping. This structural damping is also present in arrangements (b), (c), and (d) besides that due to the internal dampers.

Figure 6 shows the cross-sectional view in "POSITION 1" of the member at its midspan relative to the origin O of the x,y,z coordinate system and the proximity probe. The deviation of the cross-sectional centroid from O is due to the member imperfection which diminishes to zero at the member ends. Since the direction of the applied initial deflection (plucking) is either along Oz or parallel to it, it was decided to study the effect on the member dynamic response of the various positions of the midspan cross section as shown in figure 6. The member had a near-complete restraint with respect to axial displacement at the ends owing to the rigid test bed at the bottom and a rather rigid bracket at its top. Thus, for example, if the member was plucked along Oz with position 2 as the initial location, some small amount of axial compression was induced causing the member to vibrate outside of the plane Oz and also wobble to some extent. Although these three-dimensional effects are not accounted for in the analysis presented earlier in this memorandum, the response of the member parallel to or in line with Oz recorded experimentally compared favorably well with the corresponding analytical results as discussed later. The other imperfection positions, 3 and 4, in which the member was tested are also shown in figure 6.

Table 1 presents a summary of the results based on conducting experiments on the partially restrained member with various imperfection positions (see fig. 6) and in the absence or presence of damping devices (see fig. 5). The test results are numbered 1 through 8 each of which is an average of three separate tests. Tests 1 through 4 were conducted in the absence of damping devices for the four imperfection positions 1 through 4, respectively. The amount of structural damping was measured by the logarithmic decrement method (see ref. 6) and is summarized in appendix D as it applies to the problem under consideration. The damping ratio ζ defined in appendix D is also given in table 1 and is calculated from the experimental deflection-time response curve of the member at its midspan. The natural frequency of the member is also calculated using the same curve and is tabulated as f_e. Tests 5 and 6 were conducted with the damping device (b) shown in figure 5 with imperfection positions 1 and 4, respectively. Tests 7 and 8 were conducted with imperfection position 4, and with damping devices (c) and (d), respectively.

Effect of Imperfection on Member Vibration

In the absence of damping devices, the effect of the various imperfection positions shown in figure 6 on the member dynamic response may be observed by comparing the ζ and the f_e values for tests 1 through 4. The ζ values due to structural damping range from 0.0034 to 0.0183. The f_e values vary from 3.16 to 4.10 Hz. It should also be noted that the smallest ζ value (0.0034) among these four tests does not correspond to the maximum f_e value. It is apparent, therefore, that the effect of the imperfection position on the natural frequency of the member is significant. The axial end restraints, and three-dimensional deflection and wobbling of the member even though it is plucked only in one plane, appear to be the main causes of the observed variation in the f_e values. The dynamic spatial response of the member brings

into play the strong axis flexural stiffness of the end restraints as well as additional spatial damping effects which alter the f_e values. In the presence of damping device (b), tests 5 and 6 show that the imperfection position 4 results in higher damping and natural frequency values (e.g., larger ζ and f_e values) as compared to those for the position 1. This type of behavior may again be attributable to the attendant spatial effects.

Effectiveness of Passive Dampers

Test 4, 6, 7, and 8 were all conducted with imperfection position 4 (see table 1 and fig. 6) with damping types (a) through (d), respectively, as shown in figure 5. The ζ and f_e values are given in table 1 and the envelopes of the deflection-time response curves are presented in figure 7 in which Δ is the normalized midspan amplitude parallel to the Oz axis (see fig. 6) and t is the time in seconds. The outermost pair of curves in figure 7 represented by solid lines corresponds to damping type (a), that is, structural damping only. The curves for damping types (b), (d), and (c) are represented by dashed, dash-dot, and dash-dash-dot lines, respectively. Clearly, the damping type (c) with a lead shot at each of the locations $x = 0.25L$, $0.50L$, and $0.75L$ is the most effective of the ones considered in terms of its ability to absorb energy and thereby reduce vibration. It should be noted, however, that the damping types (c) and (d) result in nearly identical Δ-t envelopes up to about $t = 1.5$ sec, after which type (c) shows a slight superiority over type (d), although they may be considered practically the same. Furthermore, as seen from table 1, the ζ value for type (d) is greater than that for type (c) while the f_e value for type (c) is smaller than that for type (d). Again, the spatial effects may be a cause of such response.

COMPARISON OF THEORETICAL AND EXPERIMENTAL RESULTS

With relatively small values of the damping ratio ζ such as those for tests 1 through 8 given in table 1, a significant variation of the natural damped frequency of the member with ζ cannot be expected as evident from equation (16). Thus, it is concluded that the variation in f_e values as seen from table 1 is attributable primarily to the spatial effects mentioned earlier. To see how well the frequency predictions from the theoretical analyses presented earlier in this memorandum compare with those observed experimentally, the physical dimensions, the material properties, the end restraint stiffness, and the ζ values from table 1 were fed into the computer programs developed specially for this purpose. The f_e values from the exact solution, the approximate analytic solution (involving eq. (28)), and the finite-difference solution for all the eight tests were found to be 3.58, 3.63, and 3.52 Hz, respectively. The theoretical analyses were conducted on a member with no initial imperfections. These theoretical f_e values are in very good agreement with the average experimental f_e value of 3.42 Hz for the eight tests in table 1. Also, the experimental f_e values are in the range 3.16 to 4.10 Hz and all of the theoretical predictions are within this range.

A comparison of normalized deflection-time curves for a time interval of 1 sec obtained from each of the three analyses was also made to those obtained experimentally. During the time interval considered, the theoretical predictions were found to be in very good agreement with the experimental results. It should be recognized, however, that without incorporating into the theoretical analyses all of the existing spatial effects mentioned earlier, the theoretically predicted deflection-time curves will deviate from the experimental ones over longer intervals of time (such as of the order of 2 to 3 sec). That this would be the case may be seen by comparing the ζ values and

the Δ-t envelopes in figure 7 for tests 7 and 8. Any of the three theoretical analyses presented for a member without spatial effects will predict a greater decay with time of the deflections for test 8 due to its larger ζ value of 0.0354 compared to that for test 7 with a ζ value of 0.0296. The Δ-t curves for these two tests, in figure 7, show that beyond $t = 1.5$ sec approximately, the results are on the contrary. For a more accurate theoretical prediciton of the overall deflection-time response of the member, therefore, a three-dimensional analysis should be formulated.

SUMMARY AND CONCLUSIONS

The following is a brief summary and some conclusions based on the outcome of the research reported herein:

1. Explicit formulas for predicting the elastic buckling load and the natural frequency of columns with partial rotational end restraints are developed. The buckling load formula gives results nearly identical to those from the exact, and the finite element techniques. The natural frequency formula also gives results nearly identical to those from the exact analysis.

2. The natural frequency predictions from the formula developed, the exact analysis, and the finite-difference formulation presented are all in good agreement with those observed experimentally despite the presence of significant axial member end restraints and the attendant spatial effects in the member response.

3. The member deflection-time response, with a zero axial load, from the theoretical analyses is in very good agreement with that observed experimentally for about four cycles of vibration beyond which some deviation is expected due to the spatial and axial end restraint effects not included in the analyses.

4. The three lead shot configurations provided considerably greater damping than the single lead shot damper.

APPENDIX A

TERMS IN THE MATRIX OF EQUATION (21)

In this appendix, the 16 terms defining the matrix of equation (21) are given as follows:

$$a_{11} = a_{13} = 1$$

$$a_{12} = a_{14} = 0$$

$$a_{21} = - EI\beta_1^2$$

$$a_{22} = - K\beta_1$$

$$a_{23} = EI\beta_2^2$$

$$a_{24} = - K\beta_2$$

$$a_{31} = \cos \beta_1 L$$

$$a_{32} = \sin \beta_1 L$$

$$a_{33} = \cosh \beta_2 L$$

$$a_{34} = \sinh \beta_2 L$$

$$a_{41} = EI\beta_1 \cos \beta_1 L - K\beta_1 \sin \beta_1 L$$

$$a_{42} = EI\beta_1 \sin \beta_1 L + K\beta_1 \cos \beta_1 L$$

$$a_{43} = EI\beta_2^2 \cosh \beta_2 L + K\beta_2 \sinh \beta_2 L$$

$$a_{44} = EI\beta_2^2 \sinh \beta_2 L + K\beta_2 \cosh \beta_2 L$$

APPENDIX B

TERMS OF MATRIX [Γ]

As an example, the various terms of the matrix [Γ] used in equation (39) are defined in this appendix for M = 6. The various terms are as follows:

$$\Gamma_{11} = \Gamma_{55} = 6b_1 - 2b_2 - 2b_3 - b_4 - b_1 b_5$$

$$\Gamma_{12} = \Gamma_{23} = \Gamma_{34} = \Gamma_{45} = -4b_1 + b_2$$

$$\Gamma_{13} = \Gamma_{24} = \Gamma_{35} = b_1$$

$$\Gamma_{14} = \Gamma_{15} = \Gamma_{25} = 0$$

$$\Gamma_{22} = \Gamma_{33} = \Gamma_{44} = 6b_1 - 2b_2 - 2b_3 - b_4$$

$$\Gamma_{IJ} = \Gamma_{JI}$$

$$b_1 = \frac{EI}{h^4}$$

$$b_2 = \frac{P}{h^2}$$

$$b_5 = \frac{\frac{EI}{h} - \frac{K}{2}}{\frac{EI}{h} + \frac{K}{2}}$$

The terms b_3 and b_4 are defined by equations (42) and (43), respectively.

APPENDIX C

DERIVATION OF $w_{1,1}$ EXPRESSION

The $w_{1,1}$ expression given by equation (45) is derived in this appendix. With:

$$\frac{1}{\Delta t}\left[w(x_1,t_1) - w(x_1,0)\right] = \frac{\partial w}{\partial t}(x_1,0) + \frac{\Delta t}{2}\frac{\partial^2 w}{\partial t^2}(x_1,0) + \frac{(\Delta t)^2}{6}\frac{\partial^3 w}{\partial t^3}[x_1,0(\Delta t)] \tag{1}$$

suppose that equation (1) also holds on the initial line, that is,

$$EI\frac{\partial^4 w}{\partial x^4}(w_1,0) + P\left[\frac{\partial^2 w}{\partial x^2}(x_1,0) + \phi_1\right] + \rho\frac{\partial^2 w}{\partial t^2}(x_1,0) + C\frac{\partial w}{\partial t}(x_1,0) = 0 \tag{C2}$$

If $\phi(x_1)$ in equation (6) exists, then:

$$\frac{\partial^2 w}{\partial t^2}(x_1,0) = -\frac{EI}{\rho}\frac{\partial^4 w}{\partial x^4}(x_1,0) - \frac{P}{\rho}\left[\frac{\partial^2 w}{\partial x^2}(x_1,0) + \phi_1\right] - \frac{C}{\rho}\frac{\partial w}{\partial t}(x_1,0)$$

$$= -\frac{EI}{\rho}\frac{d^4}{dx^4}\phi(x_1) - \frac{P}{\rho}\left[\frac{d^2}{dx^2}\phi(x_1) + \phi_1\right] \tag{C3}$$

in which the initial condition (7) is already used. Using the central difference expressions for the second and fourth order ordinary derivatives of $\phi(x_1)$ in equation (C3) results in:

$$\frac{\partial^2 w}{\partial t^2}(x_1,0) = -\frac{EI}{\rho}\frac{1}{h^4}(\phi_{1-2} - 4\phi_{1-1} + 6\phi_1 - 4\phi_{1+1} + \phi_{1+2}) - \frac{P}{\rho}\left[\frac{1}{h^2}(\phi_{1-1} - 2\phi_1 + \phi_{1+1}) + \phi_1\right] \tag{C4}$$

Substituting equation (C4) into equation (C1), and rearranging gives:

$$w(x_i,t_1) = w(x_i,0) - \frac{(\Delta t)^2}{2h^4}\frac{EI}{\rho}\left(\phi_{i-2} - 4\phi_{i-1} + 6\phi_i - 4\phi_{i+1} + \phi_{i+2}\right)$$

$$- \frac{(\Delta t)^2}{2}\frac{P}{\rho}\left[\frac{1}{h^2}\left(\phi_{i-1} - 2\phi_i + \phi_{i+1}\right) + \phi_i\right] \qquad (C5)$$

which takes the form of equation (45) if condensed by using equations (46) through (48).

APPENDIX D

EQUATION FOR DAMPING RATIO

The logarithmic decrement method (see ref. 6) was used to calculate the damping ratio ζ defined as:

$$\zeta = \frac{C}{C_c} \tag{D1}$$

in which C is the damping coefficient and C_c is the critical damping factor given by:

$$C_c = 2\sqrt{EI\rho\lambda} \tag{D2}$$

The damping ratio was calculated using the following equation:

$$\zeta = \frac{\delta}{\sqrt{(2\pi)^2 + \delta^2}} \tag{D3}$$

in which δ is given by:

$$\delta = \ln \frac{x_1}{x_2} \tag{D4}$$

where x_1 and x_2 are the successive amplitudes of vibration as defined in reference 6. Each ζ value was obtained by taking an average of five δ values from each deflection-time plot.

REFERENCES

1. Timoshenko, S. P.; and Gere, J. M.: Theory of Elastic Stability. 2nd Edition, McGraw-Hill Book Company, New York, 1961.

2. Warburton, G. B.: The Dynamical Behavior of Structures. 2nd Edition, Pergamon Press, New York, 1976.

3. Allen, H. G.; and Bulson, P. S.: Background to Buckling. McGraw-Hill Book Company, New York, 1980.

4. Clough, R. W.; and Penzien, J.: Dynamics of Structures. McGraw-Hill Book Company, New York, 1975.

5. Harris, C. M.; and Crede, C. E.; editors: Shock and Vibration Handbook, Volume 1. McGraw-Hill Book Company, New York, 1961.

6. Thompson, W. T.: Theory of Vibration. Prentice-Hall, Inc., New Jersey, 1972.

7. Carnahan, B.; Luther, H. A.; and Wilkes, J. O.: Applied Numerical Methods. John Wiley & Sons, Inc., New York, 1969.

TABLE 1.- SUMMARY OF EXPERIMENTAL RESULTS

Number	Damping type (fig. 5)	Imperfection position (fig. 6)	ζ	f_e (Hz)
1	a	1	0.0166	3.43
2	a	2	.0049	4.10
3	a	3	.0183	3.16
4	a	4	.0034	3.51
5	b	1	.0173	3.23
6	b	4	.0053	3.45
7	c	4	.0296	3.20
8	d	4	.0354	3.30

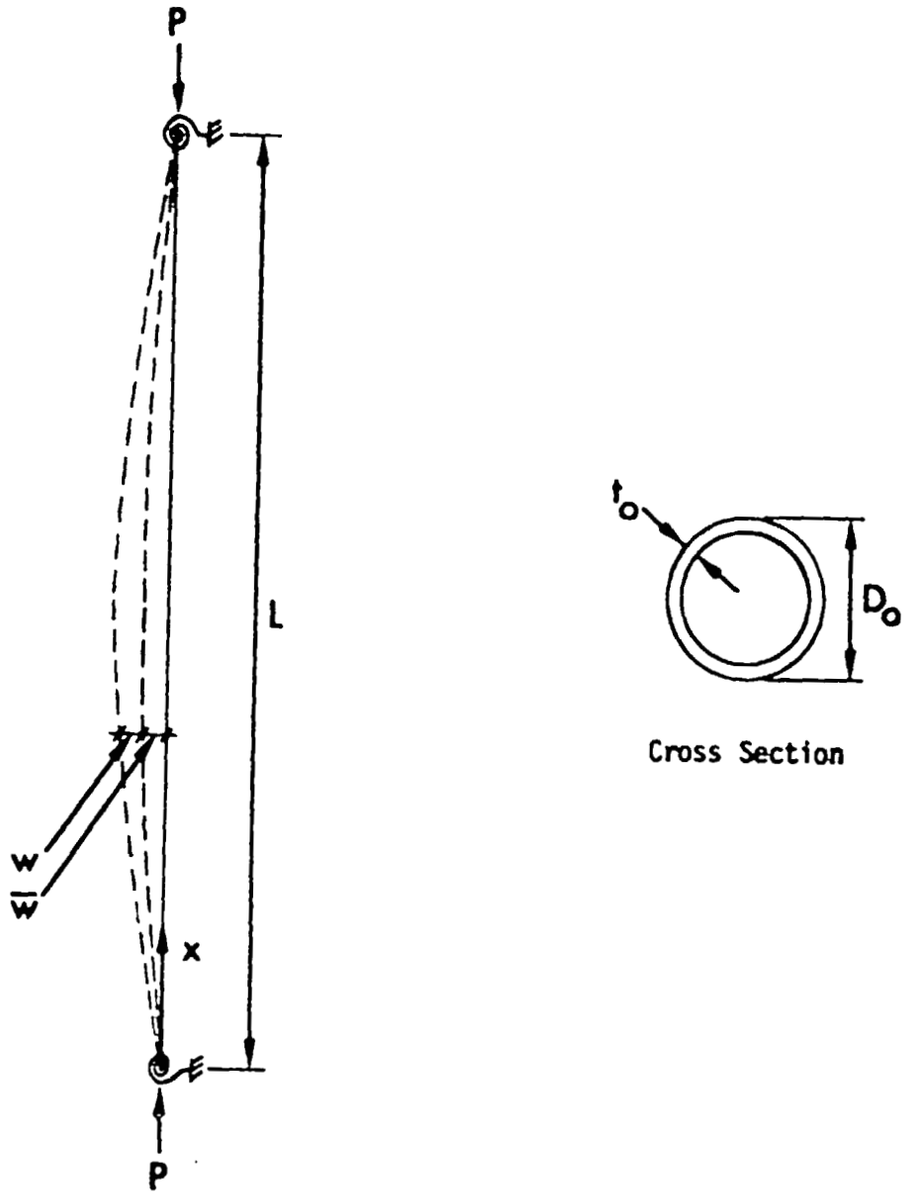

FIGURE 1 Partially Restrained Member

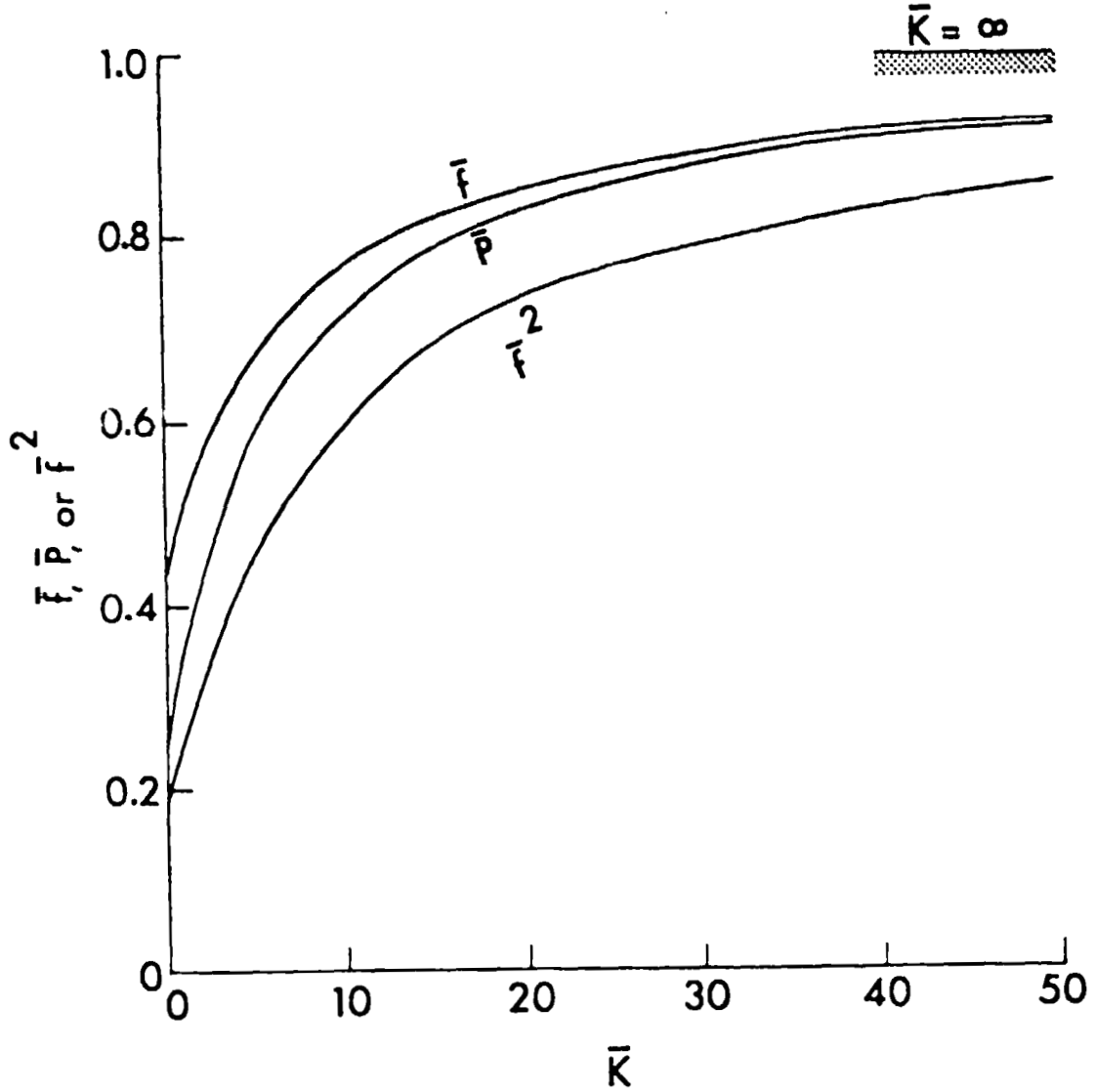

FIGURE 2 Dimensionless Interaction Curves

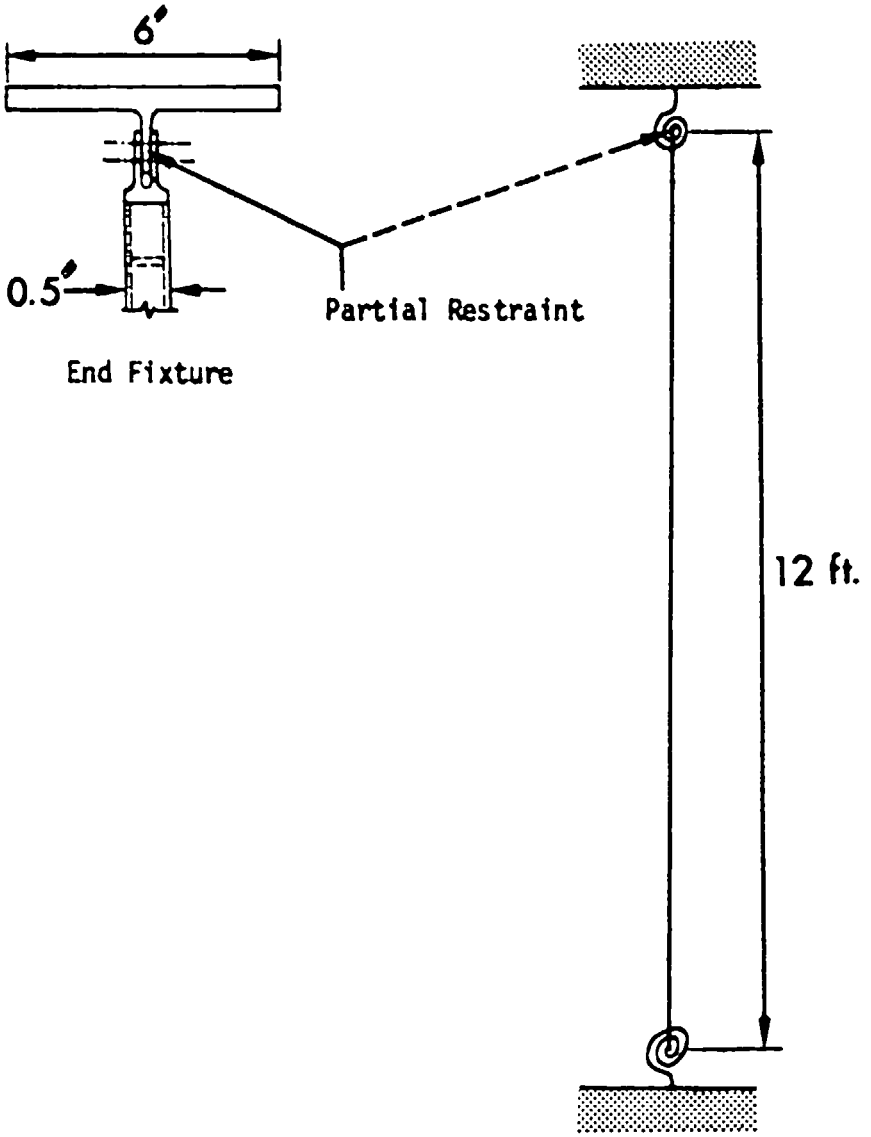

FIGURE 3 Schematic of Test Specimen and End Fixture

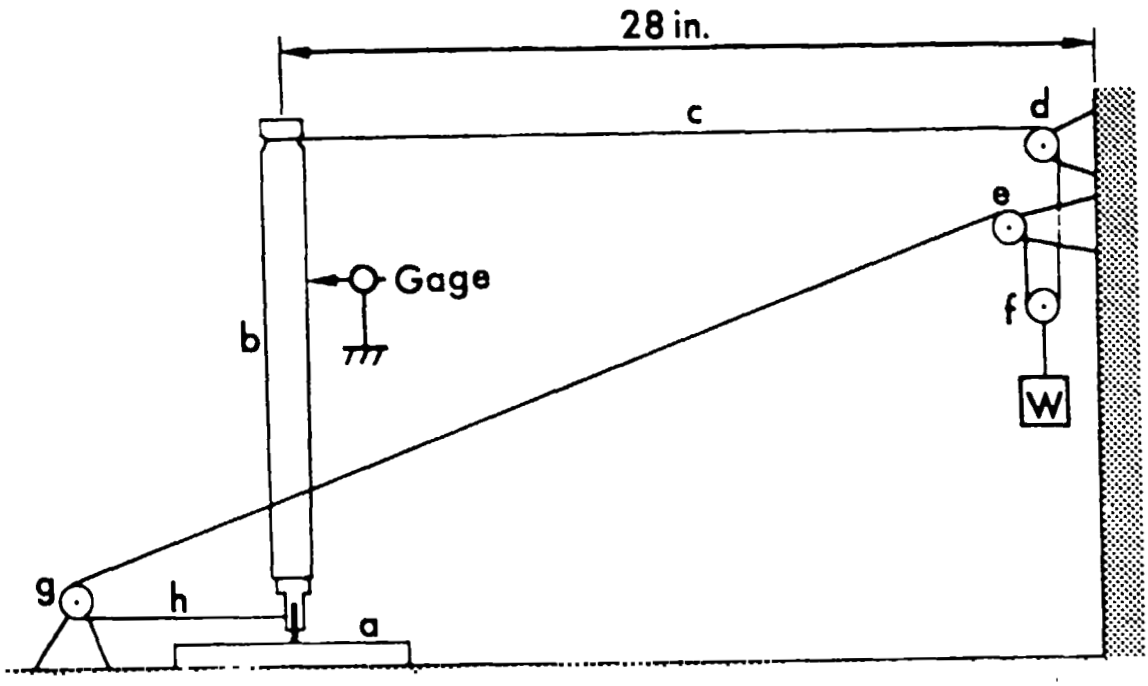

FIGURE 4 Schematic of Apparatus for Determining Restraint Stiffness

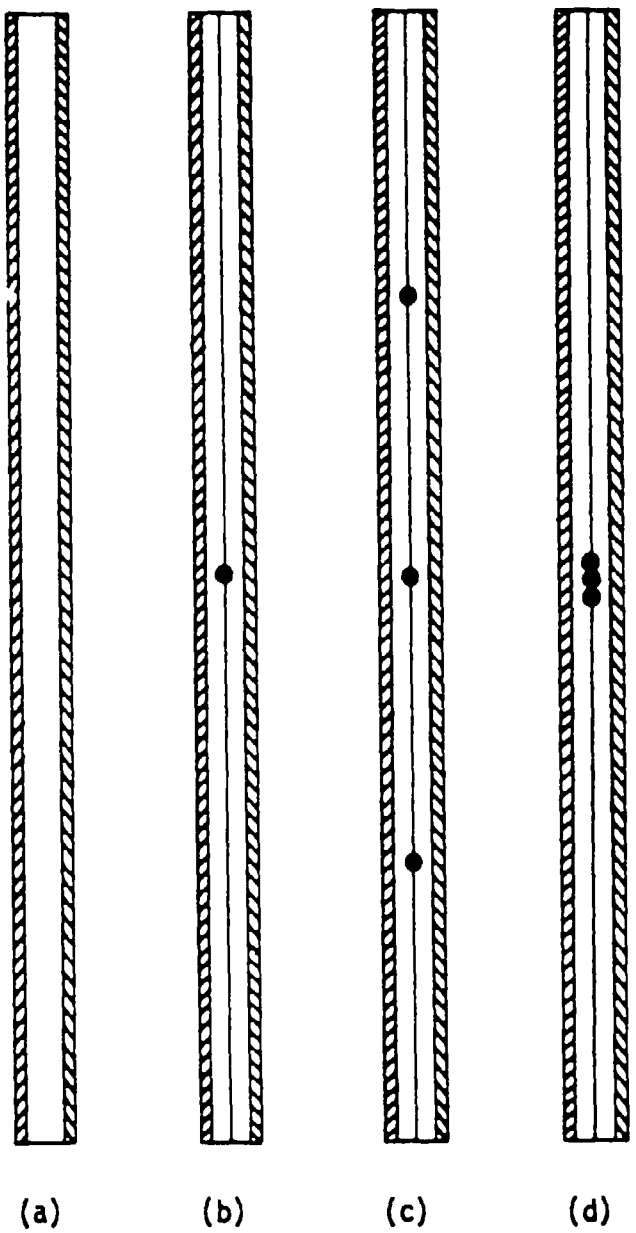

FIGURE 5 Test Specimen with Internal Dampers

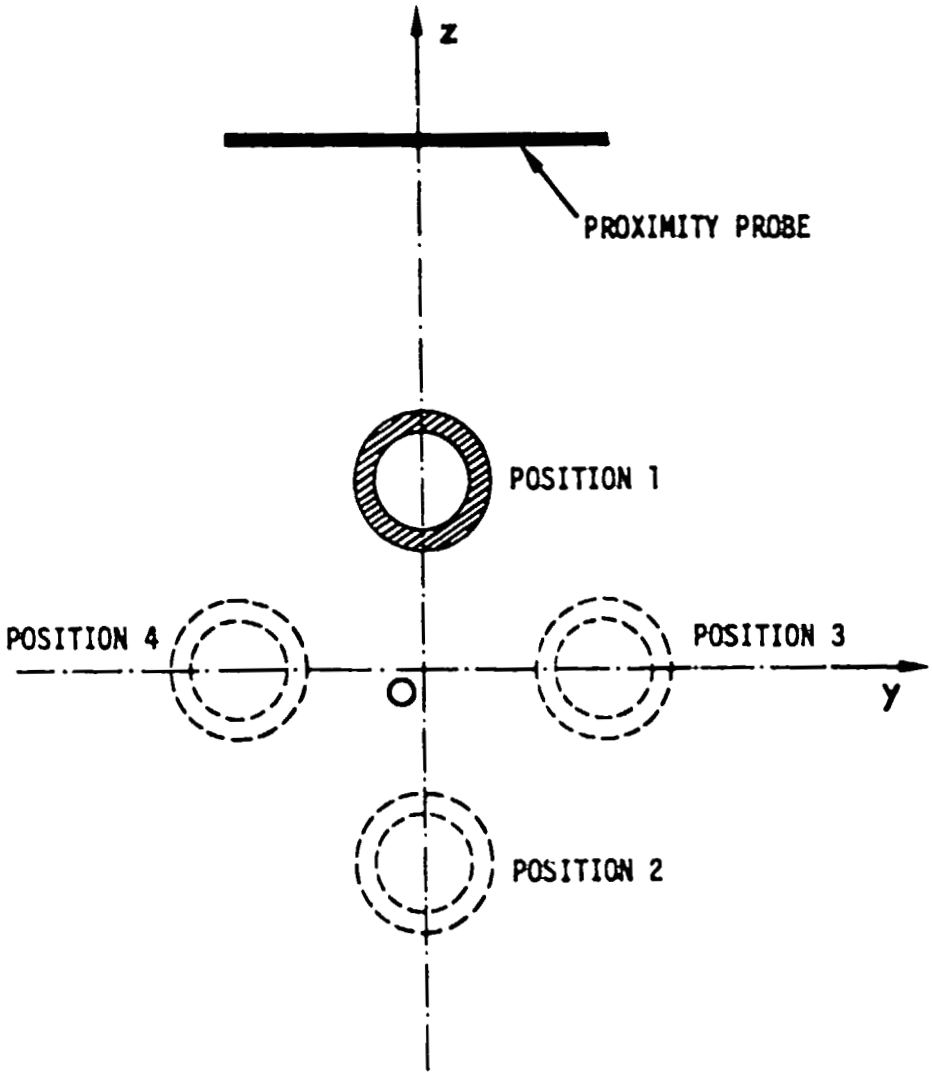

FIGURE 6 Various Imperfection Positions at Member Midspan

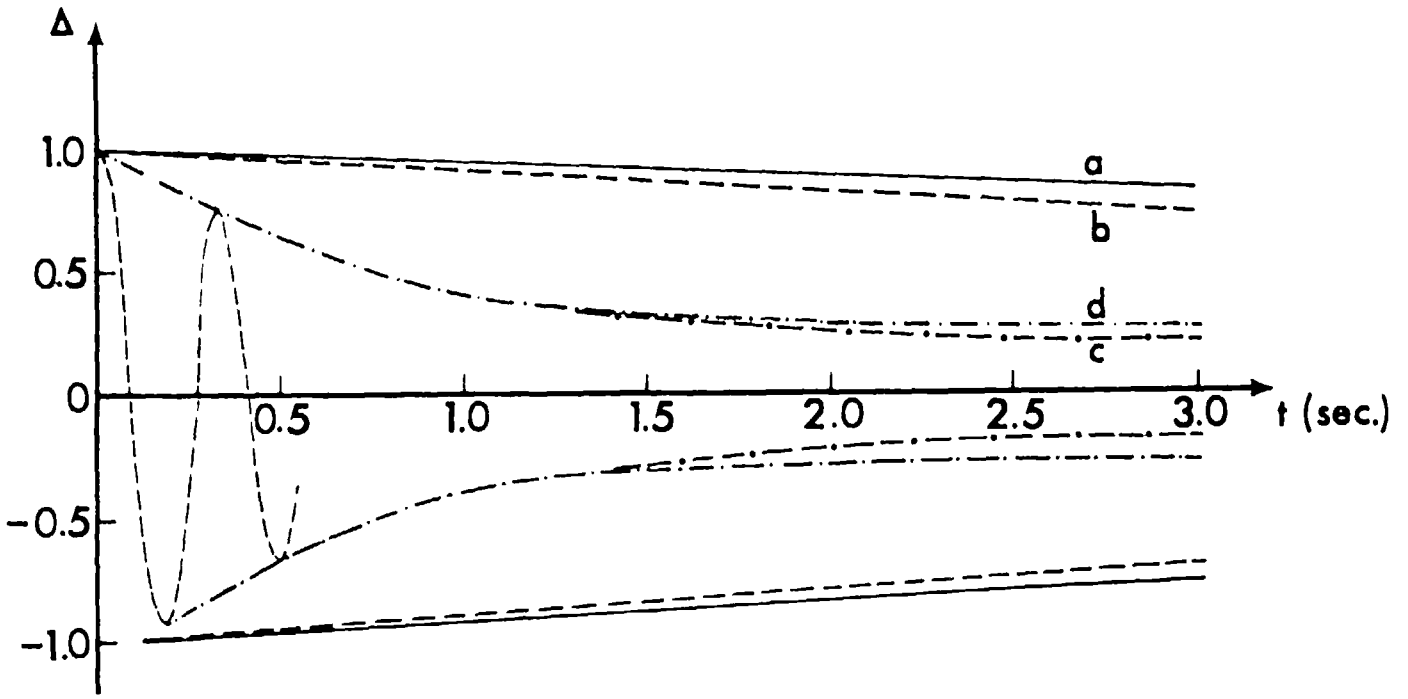

FIGURE 7 Member Dynamic Response Envelopes with Various Internal Dampers